Automatic 3D seed location and orientation in CT images for prostate brachytherapy

Huu-Giao N'Guyen, Céline Fouard, François Meneu, Jean-Yves Giraud, Jocelyne Troccaz

Automatic 3D seed location and orientation detection in CT image for prostate brachytherapy

Huu-Giao Nguyen[1], Celine Fouard[1], Francois Meneu[2], Jean-Yves Giraud[2] and Jocelyne Troccaz[1]

***Abstract*—In prostate brachytherapy, the analysis of the 3D pose information of each individual implanted seed is one of the critical issues for dose calculation and procedure quality assessment. This paper addresses the development of an automatic image processing solution for the separation, localization and 3D orientation estimation of prostate seeds. This solution combines an initial detection of a set of seed candidates in CT images (using a thresholding and connected component method) with an orientation estimation using principal components analysis (PCA). The main originality of the work is the ability to classify the detected objects based on a priori intensity and volume information and to separate groups of seeds using a modified k-means method. Experiments were carried out on CT images of a phantom and a patient aiming to compare the proposed solution with manual segmentation or other previous work in terms of detection performance and calculation time.**

I. Introduction

With an incidence rate of 152 per 100,000 men worldwide per year for 2006-2010, prostate cancer is the second most frequently diagnosed cancer in men (cf. SEER Cancer Statistics Review). The improvement of the diagnostic and therapeutic methods for prostate cancer has become increasingly important. The low-risk prostate brachytherapy treatment, that uses low dose rate radioactive seeds, is a common and highly effective method to manage localized prostate cancer. Lines of seeds, loose or stranded, are inserted through parallel needles into the prostate. In practice, the number of seeds implanted in the prostate commonly range from 40 to 100. The goal of a successful operation is to position the seeds in order to get the proper dose coverage throughout the prostate while limiting the risk for the neighboring organs. In theory, seeds are aligned in the needle insertion direction. However, in practice the seed implantation depends on many biomechanical factors as well as human experience. Hence, the seeds may be dropped out of position in spite of any special care or effort used when placing the needles and delivering the seeds. This may also result in groups of closely spaced seeds. We name such a group a *union-seed* (Fig.1). For treatment quality assessment, a CT-based post-implant dosimetry is generally performed one month after the intervention once any inflammatory modification of the prostate has disappeared. The CT examination often shows that seeds are not aligned in the implantation direction with also a possible migration of the seeds [1]. Although it has been recommended by the American Association of Physicists in Medicine [2] to determine the 3D dose distributions of brachytherapy seeds based on real seed positions and orientations, most treatment planning software still work with the assumption that all seeds are aligned with the CT axis. The optimal location and orientation of the seeds, including the ability to separate union-seeds, have therefore been reported as a major challenge for the evaluation of prostate brachytherapy [3-7].

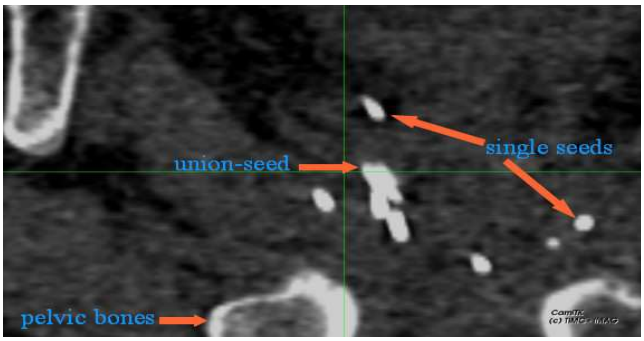

Fig. 1. Example of implanted seeds as visible in one slice of CT image.

Thus seed localization has been largely studied and published. For example, a blob detection using Laplacian of Gaussian was considered in [6] to determinate the location of seeds in IRON images (Inversion-Recovery with On-Resonant Water Suppression) with no explicit mention of the seed orientations.Wei et al [7] segmented the seeds from the subtraction map between background and post-implant ultrasound images and then applied a PCA method for orientation detection. Meaningful advances were also reported for seed localization in X-ray images such as volume reconstruction using Gaussian-blurred images in [3]. Chng et al. [4] estimated the seed orientations from the tangent vector to the curve of a seed strand identified in post-implant CT at each seed's position. A large collection of papers consider stranded seeds whose real orientation is generally closer to the planned one. These types of seeds, however, limit the clinician's ability to sculpt the dose to the treatment constraints. Moreover, these methods do not manage union-seeds.

We have begun developing post-implant image processing software at our institution, emphasizing the need for small computational complexity and high effectiveness of seed detection. In this study, we exploit the high intensity appearance of radioactive seeds in CT images for a solution based on thresholding and connected component segmentation [8]. In addition to the main objective of

*This work is supported by INSERM Dorgipro project.

(1) These authors are with UJF-Grenoble 1 / CNRS / TIMC-IMAG UMR 5525, Grenoble, F-38041, France.

(2)These authors are with Radiotherapy department, Grenoble University Hospital, 38100 Grenoble, France.

accurate seed localization and orientation, we also handle the separation of union-seeds. Here, the PCA method [9] is used for orientation estimation and the k-means segmentation method [10] is improved. This paper is organized as follows: in Section II, the materials used during this work are presented. In Section III we described the proposed solution. Evaluation is reported for datasets coming from a phantom and one anonymous patient in Section IV. We then discuss the main contributions and potential extensions of the proposed approach in Section V.

II. Materials

The clinical team of the Grenoble University Hospital uses BEBIG IsoSeed®I-125 seeds. A seed is made of a cylindrical-shaped ceramic material, saturated with radioactive iodine-125 compound and a gold marker located in the center, which are all enclosed by a laser-sealed titanium tube. The outer physical dimensions of the seed are $l=4.5\pm0.2$mm length and $r=0.4\pm0.02$mm external radius. The iodine-125 isotope emits photons at a maximum energy of 35keV and has a half-life of 59.46 days. This information is provided by the manufacturer [11].

The 3D CT images were obtained using a GE Lightspeed RT16 scanner with the default X-ray tube parameters: 120kVp, 380-440mA.s. The slice width was 0.625mm with 16frames/sec for each slice. The image reconstruction matrices were 512x512 archived in DICOM 3.0 format with 16-bit gray-level intensities.

III. Methods

A. Seed localization using connected object segmentation

The initial step consists in detecting a list of candidate seeds using segmentation methods. Numerous approaches in image processing have been proposed to segment individual objects in images, e.g. watershed transformation [12] and Level Set [13]. In this paper, the *connected component labeling* method [8] is considered because of its simplicity and its computational efficiency with only an intensity threshold parameter t. Indeed, we first threshold the original volume in accordance with a value t, then each connected component (using 26-connectivity) is assigned a label i. All the voxels corresponding to a connected component have the same label, unique to its particular component. The location of each component is determined as its center of mass c_i.

In this work, the choice of intensity threshold t can be heuristically set based on the image characteristics and the physical characteristics of the X-ray absorption of the seeds. Fig.2 shows an example of the connected components detected in the CT image of a patient. We can assume that the pelvic bones are the very large components with volumes more 100 times bigger than the real volume of the seeds (denoted as $RV=r^2\pi l$). In contrast, noise is composed of tiny components, with volumes less than one third of RV. The pelvic bones and noise are removed. The other components are kept as the candidate seeds consisting of two types: single seeds and union-seeds. The union-seeds are classified based on their volume compared to a single seed (denoted V_{single}). In practice, up to 4 or 5 seeds can be included in a union-seed. In this first stage, the union-seeds cannot be separated. In practice, the union-seeds always lead to potential inaccuracies in location and orientation estimation. Hence, we propose an extension of this method with a separation step presented in Section III.C.

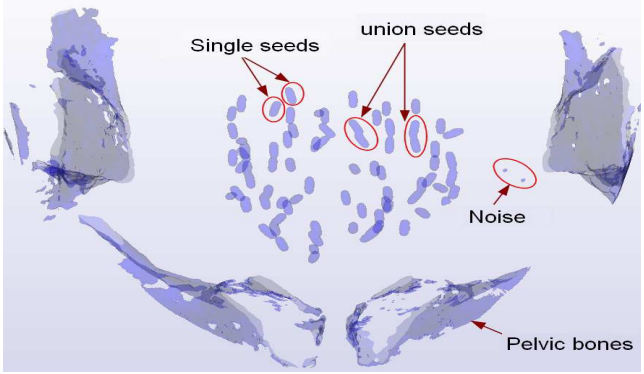

Fig. 2. Example of connected component detection in a 3D CT image with 190 objects detected using an intensity threshold of 700 (16-bit gray-level intensity).

B. Orientation estimation using PCA method

Considering the set of n detected voxels for each component, this second stage aims at estimating the 3D orientation of the components. Numerous approaches have been proposed including 3D Hough plane transforms [14] or minimal enclosing bounding boxes [15]. However, these methods are not suited for recognition in medical images because of their complexity and the high impact of image artifacts. In this work, we focused on a solution for 3D orientation estimation that would improve both aspects, by investigating the PCA method [9]. The PCA method is the simplest and most robust mathematical procedure for compressing and extracting the description of a set of correlated observations by rejecting low variance features. Considering p-dimensional feature vectors (in our case, 3D), the PCA method will be the projection of this data onto q principal components. The first principal component v_1 is the feature space along which projections have the largest eigenvalue λ_1 of the covariance matrix C of the point cloud. This is chosen as the orientation of the object. The second principal component v_2 is the direction which maximizes variance among all directions orthogonal to the first one.

C. Union-seed separation using the clustering method

Given the set of voxels of each union-seed detected by the connected component labeling, we investigate an unsupervised partitioning method using the k-means clustering method [10]. We separate the components into k single seeds by relabeling each voxel as belonging to the cluster with the nearest mean. The number k of seeds grouped in a union-seed is obtained by comparing the

component volume V to V_{single} : $k=V/V_{single}$, rounded to the nearest integer value. We first randomly select k points as the initial cluster centroids. Then, each voxel is assigned to the closest centroid. We iterate this process until all centroids do not change any more.

K-means algorithm shows its computational simplicity in many classification applications. However, there are some limitations of k-means because the resulting clusters strongly depend on the selection of the initial centroids and on size and shape differences of the regions shared by the clusters. In practice, the biggest inaccuracies of this classical k-means method occur when separating groups of parallel seeds (see Section IV). Hence, we propose an improvement to choose the initial cluster of the k-means algorithm by exploiting the information given by the PCA. We denote k-means-FS (k-means-for-seeds), the method detailed as follows. We first estimate two main directions $\{v_1,v_2\}$ of the union-seed using the PCA method. Then, (k-1) parallel planes are defined by the main direction v_1 of the union-seed and the distance $d = \lambda_2/k$ between them (see Fig.3), where λ_2 the second eigenvalue of covariance matrix C of the union-seed. These parallel planes divided the union-seed's space into k partitions. Finally, we apply the k-means clustering algorithm with the initial cluster centers that are the centroids of these k partitions.

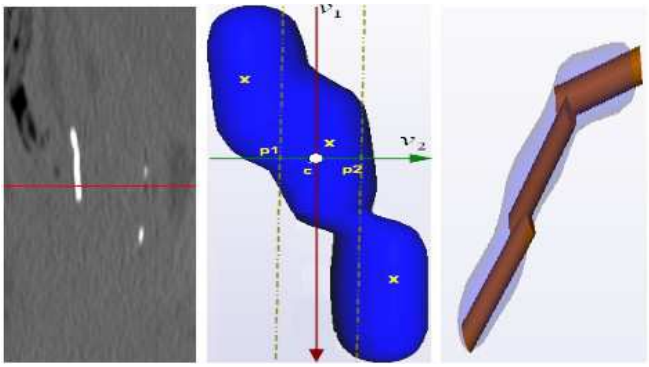

(a) (b) (c)

Fig. 3: Example of one CT slice wherein an union-seed is the longest white object (a). (b) Illustration of the choice of the initial centroid to improve the performance of k-mean method, where the crosses **x** are the centroids of k partitions, c the centroid of union-seed, $\{p_1,p_2\}$ the point used to determine the *k-1* parallel planes w.r.t the distance $d= \lambda_2/k$. (c) Obtained result.

In this work, we experimented with both the classical k-means method with different initial cluster centroids and the k-means-FS method. The cylindrical form, corresponding to the model of the seed, was reconstructed from the centroid and orientation information for each individual seed detected in the union-seed. The sum of the number of voxels common to these cylindrical forms and the union-seed was then calculated for each solution. The solution with the greatest sum was chosen as the best one.

IV. Results

A. Experimental setup

The validation of the proposed method was done using CT images of radioactive iodine-125 seeds implanted into: 1) a specially created phantom and 2) data from a real patient provided by the Grenoble University Hospital. Eleven seeds were manually positioned at the surface of the one-slab phantom (dimension 9x9x0.5cm^3). Pairs of seeds were placed in contact with each other at different orientations ranging from perpendicular to parallel, the main goal being to evaluate the ability to separate various types of union-seeds. The reference position of the seeds in the phantom was based on manual detection (Fig.4). The patient data consisted of 72 seeds implanted during a prostate brachytherapy. The CT scanner image considered in this second experiment was taken one month after the seed implantation (Fig.1). The reference position of the seeds in the prostate was manually reconstructed using clinical treatment planning software.

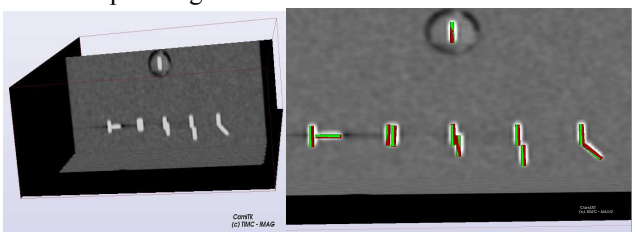

Fig. 4: 3D CT scanner image of the phantom (left) and the distribution of the 11 seeds (right): the reference position (respectively detected position) of the seeds are painted in green (respectively, red). The seeds located from left to right at the bottom are numbered from 1 to 10. The single seed on top is numbered 11.

	Image size(mm)	Voxel size(mm)	Max intensity	Min intensity
(1)	512 x 512 x 61	0.19 x 0.19 x 0.625	7431	-3024
(2)	512 x 512 x 111	0.24 x 0.24 x 0.625	6122	-3024

Table I: The characteristics of the phantom (1) and patient (2) images.

The implementation of the proposed solution was built on our open-source framework CamiTK [16] (using C++ with VTK and ITK libraries) on a 3.4GHz Intel Core i7- 2600 CPU. More information about the DICOM images can be found in Tab.I. The voxel intensity, in Hounsfield Units, for each type of material in the CT images were: phantom material *[0,400]*, patient soft tissues *[0,400]*, patient bones *[0,1350]* and seeds *[500,max]*.

In order to compare the reference location and orientation of seeds to their detected position and orientation, we used the Euclidean distance between their centroids c_1,c_2 and the dot product of their orientation vectors v_1,v_2 (Eq.1).

$$\Delta d = \sqrt{\sum_{i=1}^{3}(c_{1i}-c_{2i})^2} \qquad \Delta\theta = acos\left(\frac{v_1 \cdot v_2}{\|v_1\|\|v_2\|}\right) \quad (1)$$

where $\|v_i\|$ is the magnitude of the vector v_i, the unit of distance Δd is *mm*, and of $\Delta\theta$ is degrees.

B. Phantom experiment

Table II shows the details of the orientation difference $\Delta\theta$ and distance Δd of detected seeds compared to their reference positions using the intensity threshold t = 1400.

The best detection was obtained with the single seed no.11 where Δθ=0.23° and Δd=0.02mm. In contrast, the most difficult case for orientation estimation was the parallel union-seeds, i.e. the seeds are nearly aligned in the same orientation (in our case, seeds no.5 and 6). The greatest error in distance occurred with the "**T**" configuration, where one seed was orthogonal to the other (seeds no.1 and 2).

No.	1	2	3	4	5	6	7	8	9	10	11
Δθ°	1.13	0.68	1.10	0.72	2.25	**3.02**	0.79	0.44	1.35	1.93	**0.23**
Δd	0.14	**0.27**	0.08	0.14	0.25	0.06	0.14	0.12	0.14	0.07	**0.02**

Table II: The details of the orientation difference Δθ and distance Δd between the detected seeds and their reference positions and orientations (t=1400).

The orientation difference Δθ and distance Δd with their standard deviations are also reported in Table III for 3 different choices of the intensity threshold spanning through the range of seed intensities ([500,1400,7431]). Overall, we ran this experiment for over 20 choices of *t*. The mean distance was 0.13±0.07mm compared to 0.3mm of Chng's method [4]. The mean orientation was 1.32°±0.9 compared to 2° of Chng's method. The calculation time was 3.15s±0.3 compared to 9s of Chng's method and more than 30 minutes of manual determination of reference data. These comparisons must be interpreted carefully since the phantoms and computer systems are different. Note also that union-seed separation was not considered in Chng's method.

C. Patient experiment

Table III and Fig.5 show the results of the proposed method of seed localization in the case of a real prostate brachytherapy. All 72 seeds were detected. The best result was obtained with *t=1400*, where there was no false detection and the orientation difference and distance to their reference values were smallest. The mean calculation time was *10.1s* over 20 runs with different intensity thresholds *t*. It is a fast solution when compared to the half day of the manual detection used for the determination of reference data. From these experiment results, we suggest choosing the intensity threshold in the interval of [*1300,1700*].

	t	Δθ°	Δd (mm)	Single seeds	Union-seed	FD
(1)	600	1.47±0.8	0.14±0.06	1	5	**0**
	1400	**1.24±0.8**	0.13±0.07	1	5	**0**
	2000	1.50±0.9	**0.12±0.06**	5	3	**0**
(2)	750	3.30±1.15	0.88±0.05	64	4	34
	1100	2.40±1.10	0.81±0.06	64	4	5
	1400	**1.95±1.06**	**0.71±0.06**	64	4	**0**
	2100	2.57±1.13	1.07±0.05	66	3	**0**

Table III: The orientation difference Δθ, distance Δd with their standard deviations and the number of single seeds, union-seeds and false detection (FD) using the different choices of intensity threshold t for: phantom(1) and patient(2). The false detection will be manually deleted in our software.

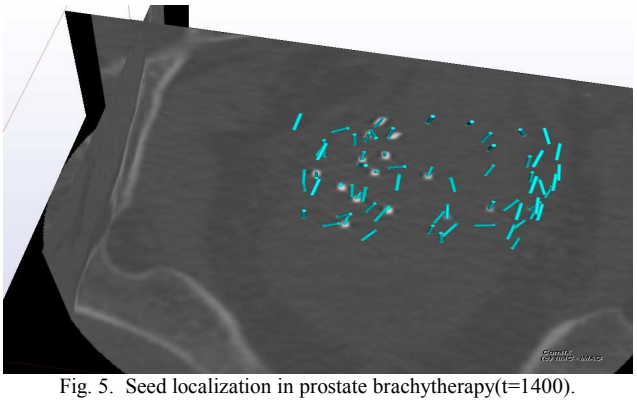

Fig. 5. Seed localization in prostate brachytherapy(t=1400).

V. Conclusion

In this study, an accurate, reliable and fast approach for location and orientation estimation of brachytherapy seeds in CT images has been presented. It also enables to automatically and reliably separate union-seeds. These results provide the potential for improving dose calculation accuracy and procedure quality assessment. The dose impact of such accuracy has still to be demonstrated and a study with this objective in mind has been launched based on a series of patients. It will be separately published. Future work will extend to an automatic choice of an optimal intensity threshold and a robust solution of seed localization for other prostate image modalities such as ultrasound.

References

[1] M. Gao et al., "Effects of seed migration on post-implant dosimetry of prostate brachytherapy," Medical Physics, vol. 34, pp. 471–481,2007.

[2] M. Rivard et al., "Update of aapm task group no. 43 report: A revised aapm protocol for brachytherapy dose calculations," Medical Physics, vol. 31(3), pp. 633–674, 2004.

[3] J. Lee et al.,"Prostate Brachytherapy Seed Localization with Gaussian Blurring and Camera Self-calibration",MICCAI, pp. 636-643, 2008.

[4] N. Chng et al., "Prostate brachytherapy postimplant dosimetry: Seed orientation and the impact of dosimetric anisotropy in stranded implants," Medical Physics, vol. 39, pp. 721–731, 2012.

[5] J. Corbett et al., "The effect of seed orientation deviations on the quality of 125i prostate implants," Medical Physics, vol. 46, pp. 2785–2800, 2001.

[6] N. Kuo et al., "Mri-based prostate brachytherapy seed localization," ISBI, pp. 1397–1400, 2010.

[7] Z. Wei et al., "Automated localization of implanted seeds in 3d trus images used for prostate brachytherapy," Medical Physics, vol. 33(7), pp. 2404–2417, 2006.

[8] L. Shapiro et al., Computer Vision. Prentice Halls, 2002, pp. 69–73.

[9] I. T. Jolliffe, Principal Component Analysis. Springer, 2002.

[10] J. Han et al., Data Mining: Concepts and Techniques. Morgan Kaufmann, 2011.

[11] IsoSeedI-125 (I25.S06) Instructions for Use, BEBIG company, 2002.

[12] L. Vincent et al., "Watersheds in digital spaces: an efficient algorithm based on immersion simulation," IEEE TPAMI, vol. 13, no. 6, pp.583–598, 1991.

[13] S. Osher et al., Geometric Level Set Methods in Imaging Vision and Graphics. Springer Verlag, 2003.

[14] W. Qiu et al., "Needle segmentation using 3d hough transform in 3d trus guided prostate transperineal therapy," Medical Physics, vol. 40,p. 042902, 2013.

[15] M. Lahanas et al., "Optimized bounding boxes for three-dimensional treatment planning in brachytherapy," Medical Physics, vol. 27, pp.2333–2342, 2000.

[16] C. Fouard et al., "CamiTK: a modular framework integrating visualization, image processing and biomechanical modeling," Soft Tissue Biomechanical Modeling for CAS, 2012, pp. 323–354.